Available online at www.sciencedirect.com
ScienceDirect
Journal of Solid State Chemistry 180 (2007) 3510–3514
JOURNAL OF SOLID STATE CHEMISTRY
www.elsevier.com/locate/jssc

Polymorphism in yttrium molybdate $Y_2Mo_3O_{12}$

Stacy D. Gates, Cora Lind*

Department of Chemistry, The University of Toledo, Toledo, OH 43606, USA

Received 3 August 2007; received in revised form 12 October 2007; accepted 14 October 2007
Available online 22 October 2007

Abstract

Yttrium molybdate ($Y_2Mo_3O_{12}$) has been prepared by non-hydrolytic sol–gel chemistry. The phase evolution upon heating was investigated using *in situ* and *ex situ* heat treatments combined with powder X-ray diffraction. This method has led to the isolation of two orthorhombic phases with different atomic connectivity. Yttrium adopts 6- and 7-coordinate sites in the *Pbcn* and *Pba*2 structures, respectively. Cocrystallization of both phases was observed in a narrow temperature range, suggesting that crystallization kinetics play a major role in phase formation. It was found that the *Pba*2 phase is the stable polymorph below 550 °C, and converts to *Pbcn* at higher temperatures.

Keywords: Yttrium molybdate; $Y_2Mo_3O_{12}$; Polymorphism; Stability; X-ray diffraction; Rietveld

1. Introduction

Within the last decade, a significant amount of research on tungstates and molybdates belonging to the $A_2M_3O_{12}$ (A = trivalent metal, M = W or Mo) family has been carried out [1–3]. This increased interest can be attributed to the discovery that various compounds in this family display negative thermal expansion (NTE) [4–9]. Thermal expansion is an intrinsic materials' property, and can lead to complications in applications that require bonding of several materials. Mismatches in thermal expansion coefficients result in device inefficiencies or failures from cracks, and stresses. Recently, NTE compounds have been used in composites to tailor the thermal expansion of a material for a specific application [10,11] while retaining the properties of the original matrix.

The $A_2M_3O_{12}$ family adopts a number of different structures. This is due to the large range of ionic radii of trivalent metals (from 0.535 Å for Al^{3+} to 1.061 Å for La^{3+}), which results in different preferences for coordination environments. Larger A^{3+} cations such as the rare-earths generally have high coordination numbers (7 or 8), while smaller cations usually form 6-coordinate structures. For most structures, the M^{6+} coordination number is four, although higher coordination numbers are possible for polymorphs with 8-coordinate trivalent metals. Trivalent metals found in the *d*- and *p*-blocks of the periodic table are most likely to form 6-coordinate compounds. There are two $A_2M_3O_{12}$ polymorphs where A is octahedrally coordinated. These 6-coordinate structures typically generate corner-sharing frameworks. The materials can crystallize in a monoclinic phase (space group $P2_1/a$), or an orthorhombic structure (space group *Pbcn*). Many compounds undergo a phase transition from the monoclinic to the orthorhombic phase upon heating. Several compounds in the $A_2M_3O_{12}$ family have been found to display NTE in the orthorhombic *Pbcn* polymorph, whereas the monoclinic structure shows positive thermal expansion. The *Pbcn* structure is also observed for the smaller lanthanides (Er–Lu) [12,13]. The 6-coordinate lanthanide and yttrium molybdates and tungstates are hygroscopic at room temperature and transform to a hydrated structure upon exposure to atmosphere [14].

Larger trivalent metals generally form structures with a 7- or 8-coordinate environment for A^{3+}. Various $A_2M_3O_{12}$ compounds belonging to the rare-earth molybdates and tungstates $Ln_2(MO_4)_3$, where M = W or Mo and Ln = La, Er, Eu, Gd, Ho, Sm, and Tb adopt orthorhombic (*Pba*2) [15–17], monoclinic ($C2/c$) [18], or tetragonal ($P42_1/m$) [13]

*Corresponding author. Fax: +1 419 530 4033.
E-mail address: cora.lind@utoledo.edu (C. Lind).

0022-4596/$ - see front matter © 2007 Elsevier Inc. All rights reserved.
doi:10.1016/j.jssc.2007.10.011

structures. Unlike the 6-coordinate structures, these $Ln_2(MO_4)_3$ compounds normally crystallize in denser, face- or edge-sharing structures.

Yttrium is often characterized as a pseudo-lanthanide, as it has very similar properties to the lanthanides. Its ionic radius is borderline between the smaller lanthanides forming the *Pbcn* structure, and those preferring structures with higher coordination numbers. Early literature states that yttrium molybdate adopts a 7-coordinate tetragonal structure at room temperature, however, no diffraction data were published [13]. A phase diagram was provided that suggested that $Y_2Mo_3O_{12}$ reversibly transforms to a 6-coordinate orthorhombic *Pbcn* polymorph above 700 °C. More recent studies assigned the structure of $Y_2Mo_3O_{12}$ to be orthorhombic in *Pbcn* at all temperatures, displaying NTE behavior between 130 and 900 °C [19]. In this paper, we report on the coexistence of $Y_2Mo_3O_{12}$ in a 7-coordinated *Pba*2 structure and a 6-coordinate *Pbcn* phase for samples prepared by a low-temperature non-hydrolytic sol–gel process. In addition, we have investigated the relative stabilities of the two phases.

2. Experimental

2.1. Materials and methods

All syntheses were carried out under argon using a non-hydrolytic sol–gel process [20]. Starting materials were purchased from Strem Chemicals (yttrium(III)chloride, molybdenum(V)chloride), Fisher Scientific (chloroform), and Sigma Aldrich (diisopropyl ether). All chemicals were stored under inert gas, and preparations were carried out under argon in dried glassware.

2.2. Synthesis

Stoichiometric quantities of YCl_3 (2 mmol) and $MoCl_5$ (3 mmol) were placed in a glass ampoule, and $CHCl_3$ (10 mL) was added to dissolve the $MoCl_5$. The solution was allowed to stir for approximately 10 min. While continuously stirring the dark brown mixture, iPr_2O (12 mmol) was added, and the mixture was stirred for an additional 10 min. The ampoule was cooled in liquid nitrogen, and sealed under vacuum. It was heated at 130 °C for 1 week. After this time, it was opened in air, and the solvent evaporated. A dark tar was recovered, which was converted to a powder by heating to 300 °C for 4 h. The powder, which was amorphous and contained residual organics, will be referred to as "raw material" for the remainder of this paper. To crystallize the sample, heat treatments were carried out in a Vecstar Furnace, model MRF1. Samples were allowed to cool in the furnace.

2.3. Characterization

Samples were characterized by thermogravimetric-differential thermal analysis (TG-DTA) and powder X-ray diffraction (XRD). Thermal analyses were carried out on a TA instruments SDT 2960 simultaneous TGA-DTA. TG-DTA data on the raw material were collected over a temperature range of 25–700 °C in air, with a heating rate of 10 °C/min. Another TG-DTA experiment, on a preheated crystalline sample, was run to 300 °C to determine the degree of hydration of the material. XRD data were collected on PANalytical X'Pert Pro and Scintag XDS-2000 diffractometers. Both instruments use Cu$K\alpha$ radiation and Bragg–Brentano geometry. The Scintag instrument is equipped with a Moxtek detector, and the PANalytical diffractometer uses an X'Celerator detector. Variable temperature XRD experiments were carried out to investigate phase evolution upon heating. The VT-XRD experiments were performed using an Anton Parr heating stage with a platinum heater strip. The VT data and air-sensitive sample holder data were acquired on the Scintag system, while all other data sets were collected on the PANalytical diffractometer. Data for phase identification were collected over the 10 to 70° angular range with a step size of 0.017° and a counting time of 5 s/step (PANalytical) or a step size of 0.02° and a scan rate of 2.0°/min (Scintag). Data for structural analysis were collected over the 10–120° angular range with a counting time of 120 s, and data for phase fraction analysis were recorded with a 0.25°/min scan rate. Rietveld refinements were carried out with the GSAS [21] and FullProf [22] program suites.

3. Results and discussion

3.1. Crystallization studies

After the recovered "tar-like" material was heated to obtain a powder, XRD revealed that the material was mainly amorphous. The few broad peaks observed for the 300 °C material were ill-defined, and could not be matched to any cards in the PDF database. Heat treatment to 500 °C resulted in an X-ray pattern that matched well with the PDF view card for orthorhombic $Tb_2Mo_3O_{12}$, which crystallizes in space group *Pba*2 with 7-coordinate Tb. A few unidentified peaks were present, and the background of the pattern suggested a contribution from an amorphous phase. The sample was heated to a higher temperature (600 °C, 3 h) in an attempt to completely crystallize the sample. The XRD data again showed the *Pba*2 phase with a few residual peaks. A final heat treatment to 700 °C revealed a different pattern with a small number of peaks and significant background contributions. The unidentified peaks in the 600 °C pattern at 18.2°, 25.5°, and 31.5° matched well with the strongest peaks in the pattern of the material heated to 700 °C (Fig. 1a and b).

In an attempt to address the phase evolution of the raw material, an *in situ* variable temperature XRD experiment was carried out. Data were collected in 100 °C intervals (room temperature to 400 °C) or 50 °C intervals (400–700 °C). To our surprise, the *Pba*2 polymorph was not observed at any temperature. Instead, crystallization of *Pbcn* $Y_2Mo_3O_{12}$ started at 450 °C. This phase could be

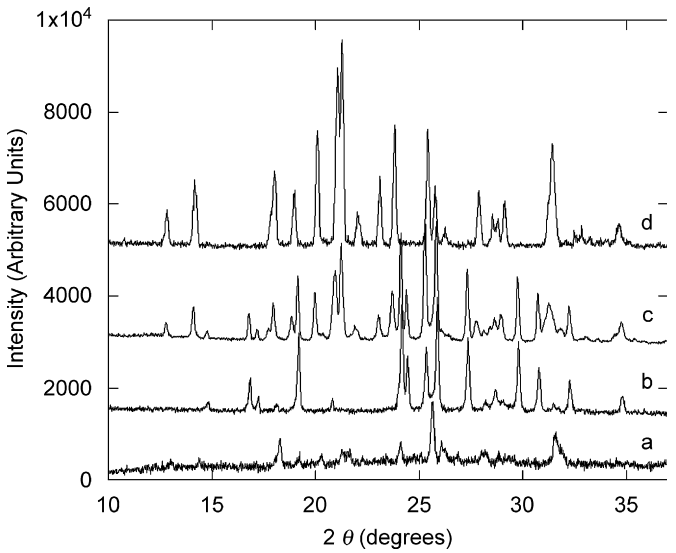

Fig. 1. X-ray diffraction patterns for various yttrium molybdate phases. (a) $Y_2Mo_3O_{12}\cdot 3H_2O$, (b) *Pba*2-$Y_2Mo_3O_{12}$ with a $Y_2Mo_3O_{12}\cdot 3H_2O$ impurity, (c) the same sample after heating to 150 °C, displaying a mixture of *Pba*2 and *Pbcn* polymorphs, and (d) *Pbcn*-$Y_2Mo_3O_{12}$ after heating to 700 °C.

quenched to room temperature. Exposure of the quenched sample to atmosphere lead to a significant change in the X-ray pattern, which resembled that of the sample recovered from 700 °C. It was found that this pattern corresponds to the trihydrate, $Y_2Mo_3O_{12}\cdot 3H_2O$, which had been previously reported [19]. According to Marinkovic et al., this trihydrate converts to the *Pbcn* structure upon heating to 130 °C, and remains in this phase up to 900 °C [19,23,24]. TG-DTA on the sample recovered from 700 °C confirmed the presence of three water molecules, which could be removed upon heating above 130 °C. After the sample was dried at 250 °C for 18 h and packed in an air-sensitive sample holder, only the orthorhombic *Pbcn* phase was observed by XRD.

A second VT-XRD experiment with 50 °C intervals was performed using a partially crystalline sample containing the *Pba*2 phase. Upon heating, coexistence of the *Pba*2 and *Pbcn* phases was observed above 100 °C (Fig. 1c), confirming the assignment of the unaccounted peaks as hydrate. No changes in the X-ray patterns were observed until about 550 °C, above which the sample converted to pure *Pbcn* (Fig. 1d). This experiment was repeated from 500 to 600 °C in 10 °C intervals to get a more precise phase transition temperature. The *Pba*2 phase was present up to 550 °C, and converted to *Pbcn* at 560 °C.

It has not been possible to obtain phase pure *Pba*2-$Y_2Mo_3O_{12}$ to date. All samples contain varying amounts of either *Pbcn*-$Y_2Mo_3O_{12}$ (dried samples protected from atmospheric moisture) or $Y_2Mo_3O_{12}\cdot 3H_2O$ (samples exposed to atmosphere).

3.2. Structural analysis

The two $Y_2Mo_3O_{12}$ polymorphs were characterized by Rietveld analysis. For all refinements, the background, histogram scale, phase fractions (for mixed phase samples), peak shape parameters, lattice constants, atomic positions, and atomic displacement parameters were varied. Results from the two refinements are given in Table 1.

The pattern of the *Pbcn* polymorph matched well with X-ray patterns previously reported for orthorhombic $Y_2Mo_3O_{12}$, and a Rietveld refinement starting with the published structure gave an excellent fit ($\chi^2 = 1.8$, $R_{Bragg} = 0.069$). The extracted lattice constants $a = 13.870$ Å, $b = 9.939$ Å, and $c = 10.023$ Å compare well with literature data ($a = 13.869$ Å, $b = 9.935$ Å, and $c = 10.022$ Å) [19]. The structure is depicted in Fig. 2a). The framework is composed of corner-sharing YO_6 octahedra and MoO_4 tetrahedra. Each YO_6 octahedron is connected to six MoO_4 octahedra, and each MoO_4 octahedron is bonded to four YO_6 octahedra. The polyhedra are slightly distorted, with Y–O bond distances ranging from 2.17 to 2.31 Å and Mo–O bond distances between 1.66 and 1.84 Å. This type of framework is typical for many NTE materials, in which the corner-sharing polyhedra give rise to the transverse vibrational motions of oxygen atoms that result in an overall contraction of the unit cell with increasing temperature.

To address the structure of the new $Y_2Mo_3O_{12}$ polymorph, Rietveld analysis was carried out on a sample that was composed of the *Pba*2 phase with a small trihydrate impurity. The crystal structure of $Gd_2Mo_3O_{12}$ [16] was used as a starting model, the initial lattice constants were estimated from selected reflections using the indices reported for $Gd_2Mo_3O_{12}$. The $Y_2Mo_3O_{12}\cdot 3H_2O$ phase was refined in Le Bail mode, as no structure has been published, and it is only an impurity phase. A Rietveld fit was carried out for the *Pba*2 polymorph. The refinement converged with $\chi^2 = 1.8$ and $R_{Bragg} = 0.085$. The extracted lattice constants were $a = 10.331$ Å, $b = 10.310$ Å, and $c = 10.564$ Å. The close values for a and b lattice constants could be the reason why the material was originally reported as tetragonal [13]. Table 2 lists the refined atomic coordinates of the new $Y_2Mo_3O_{12}$ phase. Fig. 2b shows the unit cell of *Pba*2-$Y_2Mo_3O_{12}$ viewed along the z-axis. This polymorph contains MoO_4 tetrahedra, which share corners with four YO_7 polyhedra. Each YO_7 polyhedron shares five corners with MoO_4 tetrahedra, while the last two vertices connect two yttrium centered

Table 1
Rietveld refinement results for the *Pbcn*- and *Pba*2-polymorphs of $Y_2Mo_3O_{12}$

Chemical formula	$Y_2Mo_3O_{12}$	$Y_2Mo_3O_{12}$
Space group	*Pbcn*	*Pba*2
a (Å)	13.844	10.331
b (Å)	9.926	10.310
c (Å)	10.017	10.564
V (Å^3)	1376	1125
Z	8	8
ρ (g/cm^3)	6.35	7.76
χ^2	1.8	1.8
R_{Bragg}	0.069	0.085
# variables	37	70

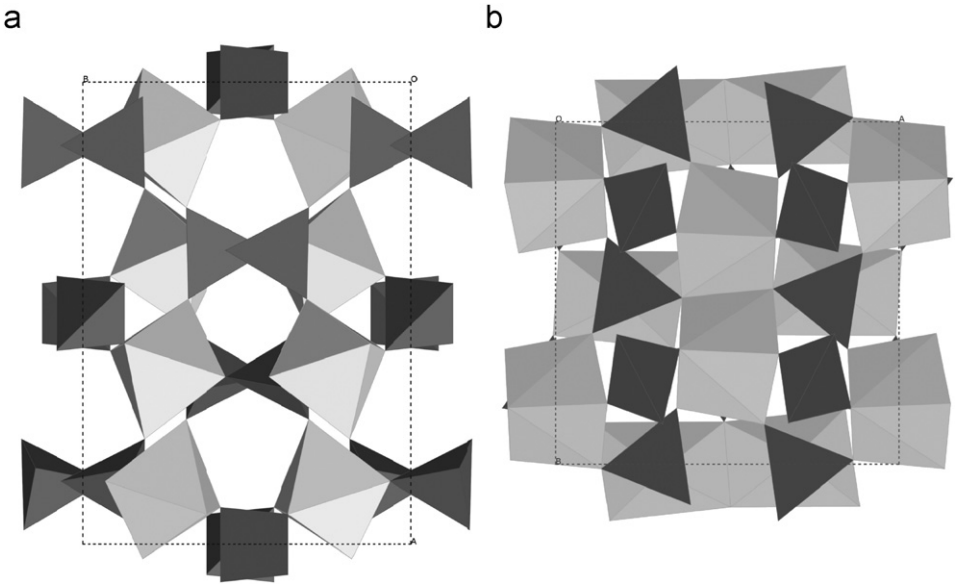

Fig. 2. Crystal structures of the (a) *Pbcn* and (b) *Pba*2 polymorphs of $Y_2Mo_3O_{12}$ viewed down the *z*-axis. Dark tetrahedra are MoO_4 units, and light polyhedra represent 6- and 7-coordinate yttrium, respectively. Polyhedra are only connected via corner-sharing in the *Pbcn* structure, while edge-shared YO_7-units are present in the *Pba*2 polymorph.

Table 2
Atomic positions for *Pba*2-$Y_2Mo_3O_{12}$

Name	*x*	*y*	*z*
Y1	0.1864(10)	0.5015(22)	0.739(93)
Y2	0.4999(28)	0.3139(10)	0.262(93)
Mo1	0.2028(10	0.4913(19)	0.354(93)
Mo2	−0.0003(30)	0.2070(10)	0.639(93)
Mo3	0.2544(22)	0.2471(22)	−0.004(93)
O1	0.1973(5)	0.5230(6)	0.537(9)
O2	0.4917(10)	0.3041(4)	0.486(9)
O3	0.1327(5)	0.0127(11)	0.316(9)
O4	0.5089(15)	0.1241(5)	0.698(9)
O5	0.1558(7)	0.1637(7)	0.684(9)
O6	0.1490(8)	0.3357(7)	0.314(9)
O7	0.3854(6)	0.3787(7)	0.729(9)
O8	0.3928(6)	0.1167(7)	0.299(9)
O9	0.1397(9)	0.1649(9)	0.105(9)
O10	0.3225(9)	0.1202(10)	0.904(9)
O11	0.3504(8)	0.3222(9)	0.094(9)
O12	0.1878(10)	0.3821(9)	0.903(9)

polyhedra in an edge-sharing fashion, resulting in Y_2O_{12} units. Y–O bond distances range from 2.13 to 2.53 Å, and Mo–O bonds are between 1.62 and 1.96 Å. This structure has a much higher density than the *Pbcn* polymorph (*Pba*2: 7.76 g/cm^3, *Pbcn*: 6.35 g/cm^3), and lacks the structural flexibility required for transverse vibrational modes resulting in NTE. *Pba*2-$Y_2Mo_3O_{12}$ is isostructural to orthorhombic $Gd_2Mo_3O_{12}$ and orthorhombic $Tb_2Mo_3O_{12}$, which exhibit the same atomic connectivity (face-shared A_2O_{12} and corner-connected MoO_4 units) with slightly less distorted polyhedra. Bond distances of the MoO_4 tetrahedra fall between 1.73 and 1.80 Å, and the bonds in the AO_7 polyhedra range from 2.26 to 2.44 Å.

3.3. Relative stabilities

The atomic connectivities in the *Pba*2 and *Pbcn* polymorphs are very different (Fig. 2). This makes interconversion between the two structures unfavorable at low temperatures, and can result in the isolation of metastable phases through preferable crystallization kinetics. The *Pba*2 polymorph could not be observed *in situ* when the raw sample was heated on the platinum strip. In addition, there was a 50 °C temperature offset between the conversion *in situ* (550 °C) and the temperature of the heat treatment of the *ex situ* sample (recovered from 600 °C). These observations suggested that the *Pbcn* polymorph is kinetically preferred, while the *Pba*2 phase was formed during the annealing process when the sample was allowed to slowly cool inside the furnace. To confirm this hypothesis, a mixed phase sample was heated to 500 °C on the heater strip for 60 h, and consecutive X-ray scans were collected. The X-ray patterns showed a very small increase in the intensity of the *Pba*2 peaks. An *ex situ* experiment was carried out by heating a sample to 530 °C in a furnace for 10 days. Refinement quality X-ray scans were collected before and after the heat treatment in an air-sensitive sample holder to prevent hydration of the *Pbcn* polymorph. Rietveld analysis showed that the sample before heat treatment contained a mixture of 72% of the *Pbcn* and 28% of the *Pba*2 phase. This ratio changed to 66% *Pbcn* and 34% *Pba*2 after the 10-day anneal at 530 °C. This shows that the *Pba*2 polymorph is more stable than the *Pbcn* structure at 530 °C (Fig. 3).

4. Conclusions

Yttrium molybdate prepared by a NHSG route shows coexistence of orthorhombic *Pba*2 and *Pbcn* polymorphs

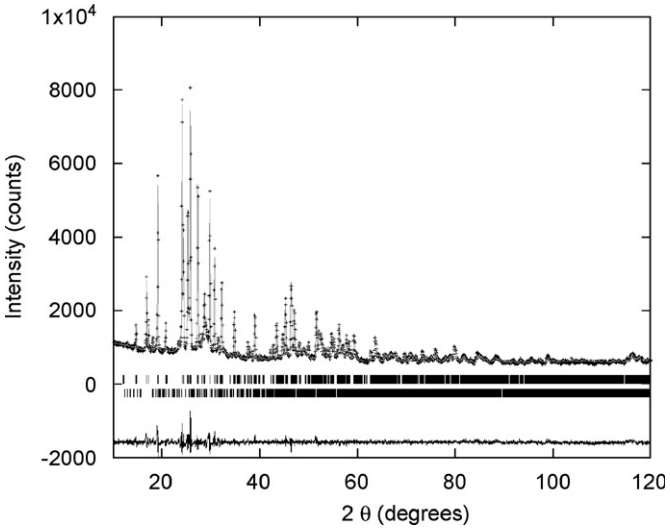

Fig. 3. Rietveld refinement of *Pba*2-$Y_2Mo_3O_{12}$ with a small $Y_2Mo_3O_{12} \cdot 3H_2O$ impurity. Crosses represent data points, and the solid line corresponds to the calculated pattern. A difference curve is shown below the tick marks (top: *Pba*2-$Y_2Mo_3O_{12}$, bottom: $Y_2Mo_3O_{12} \cdot 3H_2O$), which indicate calculated positions for Bragg reflections.

when heated to temperatures between 500 and 550 °C. The *Pba*2 phase is a new $Y_2Mo_3O_{12}$ polymorph, and was obtained during *ex situ* heat treatments through annealing. Attempts to obtain this phase during *in situ* experiments were unsuccessful. *Pba*2-$Y_2Mo_3O_{12}$ is isostructural to orthorhombic $Gd_2Mo_3O_{12}$. *Pbcn*-$Y_2Mo_3O_{12}$ readily converts to a trihydrate upon exposure to atmosphere, this hydration is reversible upon heating. It was found that the crystallization of *Pbcn* is kinetically preferred at low temperatures over formation of the *Pba*2 structure, which appears to be the thermodynamically stable polymorph below 550 °C. The *Pbcn* phase can be converted to *Pba*2 by annealing below this temperature, but the conversion is very slow. The slow kinetics explain why the *Pba*2 structure has not been observed by previous researchers, who reported *Pbcn* as the stable polymorph above 130 °C. The fact that the NTE phase is not stable below 550 °C has important implications for potential applications of this material in composites.

References

[1] A.W. Sleight, Inorg. Chem. 37 (1998) 2854.
[2] J.S.O. Evans, T.A. Mary, A.W. Sleight, Physica B 241 (1997) 311.
[3] A.K. Tyagi, S.N. Achary, M.D. Mathews, J. Alloys Compd. 339 (2002) 207.
[4] J.S.O. Evans, T.A. Mary, A.W. Sleight, J. Solid State Chem. 133 (1997) 580.
[5] T.A. Mary, A.W. Sleight, J. Mater. Res. 14 (1999) 912.
[6] A.W. Sleight, Curr. Opin. Solid State Mater. Sci. 3 (1998) 128.
[7] J.S.O. Evans, J. Chem. Soc. Dalton Trans. 19 (1999) 3317.
[8] J.S.O. Evans, T.A. Mary, Int. J. Inorg. Mater. 2 (2000) 143.
[9] J.S.O. Evans, T.A. Mary, A.W. Sleight, J. Solid State Chem. 137 (1998) 148.
[10] L.M. Sullivan, C.M. Lukehart, Chem. Mater. 17 (2005) 2136.
[11] D.A. Fleming, D.W. Johnson, P.J. Lemaire, US Patent 5,694,503, 1997.
[12] K. Nassau, H.J. Levinstein, G.M. Loiacono, Phys. Chem. Solids 26 (1965) 1805.
[13] K. Nassau, J.W. Shiever, E.T. Keve, J. Solid State Chem. 3 (1971) 411.
[14] S. Sumithra, A.M. Umarji, Solid State Sci. 8 (2006) 1453.
[15] H.J. Borchardt, J. Appl. Phys. 38 (1967) 2057.
[16] W. Jeitschko, Acta Crystallogr. B 28 (1972) 60.
[17] E.T. Keve, S.C. Abrahams, J.L. Bernstein, J. Chem. Phys. 54 (1971) 3185.
[18] M. Gartner, D. Abeln, A. Pring, M. Wilde, A. Reller, J. Solid State Chem. 111 (1994) 128.
[19] B.A. Marinkovic, P.M. Jardim, R.R. de Avillez, F. Rizzo, Solid State Sci. 7 (2005) 1377.
[20] R. Corriu, D. Leclercq, P. Lefevre, P.H. Mutin, A. Vioux, Chem. Mater. 4 (1992) 961.
[21] A.C. Larson, R.B. Von Dreele, General Structure Analysis System (GSAS), 2000, Los Alamos, 1985–2000.
[22] J. Rodriguez-Carvajal, In: Satellite Meeting on Powder Diffraction of the XV Congress of the IUCr Toulouse, France, 1990, p. 127.
[23] D. Sumithra, A. M Umarji, Mater. Res. Bull. 40 (2005) 167.
[24] T.N. Kol'tsova, Inorg. Mater. 37 (2001) 1175.